



Topological semimetal in a Bi-Bi₂Se₃ infinitely adaptive superlattice phase

T. Valla,^{1,*} Huiwen Ji,² L. M. Schoop,² A. P. Weber,^{3,4} Z.-H. Pan,¹ J. T. Sadowski,⁵ E. Vescovo,³ A. V. Fedorov,⁶ A. N. Caruso,⁴ Q. D. Gibson,² L. Muechler,⁷ C. Felser,^{7,8} and R. J. Cava^{2,†}

¹*Condensed Matter Physics and Materials Science Department, Brookhaven National Laboratory, Upton, New York 11973, USA*

²*Department of Chemistry, Princeton University, Princeton, New Jersey 08544, USA*

³*National Synchrotron Light Source, Brookhaven National Laboratory, Upton, New York 11973, USA*

⁴*Department of Physics, University of Missouri-Kansas City, Kansas City, Missouri 64110, USA*

⁵*Center for Functional Nanomaterials, Brookhaven National Laboratory, Upton, New York 11973, USA*

⁶*Advanced Light Source, Lawrence Berkeley National Laboratory, Berkeley, California 94720, USA*

⁷*Institut für Anorganische und Analytische Chemie, Johannes Gutenberg-Universität, 55128 Mainz, Germany*

⁸*Max-Planck-Institut für Chemische Physik fester Stoffe, 01187 Dresden, Germany*

(Received 12 August 2012; revised manuscript received 18 November 2012; published 5 December 2012)

We report spin- and angle-resolved photoemission studies of a topological semimetal from the infinitely adaptive series between elemental Bi and Bi₂Se₃. The compound, based on Bi₄Se₃, is a 1:1 natural superlattice of alternating Bi₂ layers and Bi₂Se₃ layers; the inclusion of S allows the growth of large crystals, with the formula Bi₄Se_{2.6}S_{0.4}. The crystals cleave along the interfaces between the Bi₂ and Bi₂Se₃ layers, with the surfaces obtained having alternating Bi or Se termination. The resulting terraces, observed by photoemission electron microscopy, create avenues suitable for the study of one-dimensional topological physics. The electronic structure, determined by spin- and angle-resolved photoemission spectroscopy, shows the existence of a surface state that forms a large, hexagonally shaped Fermi surface around the Γ point of the surface Brillouin zone, with the spin structure indicating that this material is a topological semimetal.

DOI: [10.1103/PhysRevB.86.241101](https://doi.org/10.1103/PhysRevB.86.241101)

PACS number(s): 74.25.Kc, 71.18.+y, 74.10.+v, 74.25.Jb

Three-dimensional (3D) topological insulators (TIs) have Dirac-like surface states in which the spin of the electron is locked perpendicular to its momentum in a chiral spin structure where electrons with opposite momenta have opposite spins.^{1–8} The number of experimentally identified 3D TIs has grown since the initial discovery, now including the Bi_{1–x}Sb_x alloy,³ Bi₂Se₃ and Bi₂Te₃ and their mixed anion variants,^{6,7,9–11} GeBi₂Te₄ and its PbSe-Bi₂Se₃ variants,^{9,12} TlBiSe₂,^{13,14} and SnTe.¹² Of these materials, Bi₂Se₃ has been highlighted as a model system due to its large bulk gap and simple surface electronic structure—a single Dirac-like topological surface state (TSS) whose Dirac point resides inside the gap, essentially fully spin polarized and robust against the elastic scattering and scattering on phonons.^{4,8,15–19}

Bi₂Se₃ is actually only one member of a family of compounds, called an “infinitely adaptive series,” between pure Bi metal and Bi₂Se₃, made by stacking integer numbers of bismuth bilayers and Bi₂Se₃ layers, in compounds of the type (Bi₂)_m(Bi₂Se₃)_n.²⁰ Given the topological properties of the surface of Bi₂Se₃, and the fact that the bismuth bilayer has been predicted to be a two-dimensional quantum spin Hall system,²¹ it is of interest to determine whether the superlattice material also has topological surface states. Thus far, however, these materials have been studied only structurally as small crystals, or in polycrystalline form.²⁰ Here we report the successful growth of large single crystals of the simplest member of the infinitely adaptive series, i.e., Bi₄Se₃ ($m = n = 1$), stabilized for crystal growth by partial S substitution for Se, and present spin- and angle-resolved photoemission spectroscopy (SARPES) studies of its surface electronic structure. Our measurements reveal a hexagonally shaped surface state whose spin structure indicates that Bi₄Se₃ is a semimetal that supports topological surface states. The compound is the natural bulk analog of a

recently described artificial material made by Bi adsorption on the surface of Bi₂Te₃.²² Photoemission electron microscopy (PEEM) reveals that the material cleaves with mixed Bi-layer and Se-layer terminations of the exposed terraces. This prohibits the association of the TSS with either the Bi or Se terraces by (S)ARPES, but it suggests that this material offers the unique opportunity for studying novel 1D topological physics near the terrace steps by nanometer-scale probes.

High purity elemental Bi (99.999%), Se (99.999%), and S (99.999%) were used for the Bi₄Se_{2.6}S_{0.4} crystal growth, with a starting formula of Bi_{4.5}Se₂S; the excess bismuth was used as a flux and the S greatly enhances the selective crystal growth of the 4:3 phase. The precleaned elements were sealed in clean quartz ampoules, heated to 850 °C for 1 day, and cooling over the period of 1 h to 700 °C. The crystal growth involved cooling from 700 to 550 °C over a period of 25 h, followed by centrifuging. Single crystals up to 1 cm² area in the basal plane and several millimeters thick were obtained, with high-luster cleavage faces. Single crystal x-ray diffraction data was collected on a Bruker APEX II diffractometer using Mo $K\alpha$ radiation at room temperature. Unit cell determination and refinement, and data integration were performed with Bruker APEX2 software. The crystal structure was determined using SHELXL-97 implemented through WinGX.

The ARPES experiments were carried out on a Scienta SES-100 electron spectrometer at beamline 12.0.1 of the Advanced Light Source. The spectra were recorded at photon energies ranging from 35 to 100 eV, as indicated in the text, with a combined instrumental energy resolution of ~ 12 meV and an angular resolution of better than $\pm 0.07^\circ$. Samples were cleaved at low temperature (15–20 K) under ultrahigh vacuum (UHV) conditions. The temperature was measured using a silicon sensor mounted near the sample. The SARPES

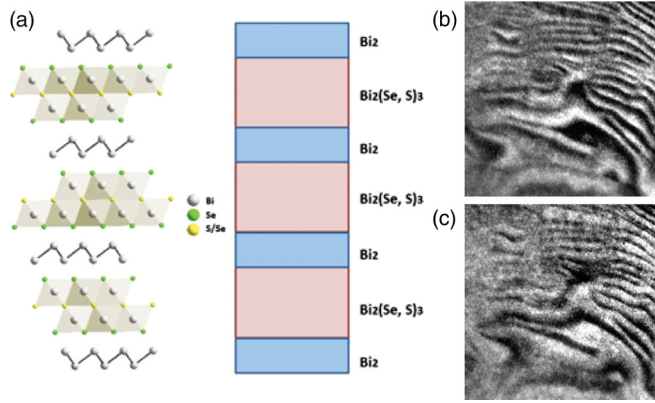


FIG. 1. (Color online) Crystal structure (a) and PEEM images of a $\text{Bi}_4\text{Se}_{2.6}\text{S}_{0.4}$ surface, taken at the Bi $5d$ (b) and Se $3d$ (c) core levels with 100 eV photons. Field of view in the PEEM images is $20 \times 20 \mu\text{m}$. Bright (dark) contours reflect regions of high (low) photoemission intensities.

experiments were performed at beamline U5UA at the National Synchrotron Light Source using a Scienta R4000 electron analyzer coupled to a pair of mini-Mott spin polarimeters that enable measurements of both the in-plane and out-of-plane spin polarizations. The spin-resolved data were recorded at 58 eV photon energy, with the sample kept at ~ 300 K. Energy and angle resolution were approximately 40 meV and 0.5° , respectively. Photoemission electron microscopy (PEEM) experiments were carried out at the x-ray PEEM (XPEEM)/low-energy EM (LEEM) end station at the National Synchrotron Light Source beamline U5UA at room temperature, with 100 eV photons using an Elmitec spectroscopic photoemission (SPE)-LEEM III microscope. All the samples were cut from the same bulk piece and cleaved and measured in ultrahigh vacuum conditions (base pressure better than 2×10^{-9} Pa in the ARPES and SARPES chambers and better than 2×10^{-8} Pa in the PEEM chamber).

Electronic structure calculations were performed in the framework of density functional theory (DFT) using the WIEN2K²³ code with a full-potential linearized augmented plane-wave and local orbitals basis^{24–26} together with the Perdew-Burke-Ernzerhof parametrization²⁷ of the generalized gradient approximation for the exchange-correlation functional. The plane wave cutoff parameter $R_{\text{MT}}K_{\text{MAX}}$ was set to 7 and the irreducible Brillouin zone (BZ) was sampled by 288 k points. Spin-orbit coupling (SOC) was included. For Bi_4Se_3 the reported crystal structure²⁸ was used. To estimate the effect of the partial S substitution for Se, electronic structure

calculations were also performed for $\text{Bi}_4\text{Se}_2\text{S}$. For this material a fully ordered structure was taken (with S fully occupying the middle layer in the quintuple layer part of the structure) and the lattice constants were interpolated linearly, according to Vegard's law,²⁹ using our data for the structure of $\text{Bi}_4\text{Se}_{2.6}\text{S}_{0.4}$.

Figure 1 shows a schematic view of the crystal structure of $\text{Bi}_4\text{Se}_{2.6}\text{S}_{0.4}$ and PEEM images of a cleaved surface. The crystal structure of the material was determined quantitatively by least squares structure analysis of a single crystal. The details of the structural characterization are given in Table I; the structure determination was used to precisely define both the crystal structure and the composition. The two PEEM micrographs show the same spot on the surface recorded at two different kinetic energies of photoelectrons, corresponding to the higher $5/2$ component of the Bi $5d$ [see Fig. 2(a)] and Se $3d$ core levels. The inversion of contrast indicates that the surface consists of alternating Bi_2 and Se terminated terraces. The terrace width is of the order of $1 \mu\text{m}$. We also note that the lower $5/2$ Bi $5d$ component and the valence band (at ~ 0.5 eV below the Fermi level) PEEM micrographs have the same contrast as the Se $3d$ core level, indicating that these features are related to the Se-terminated terraces. As the photon spot sizes in our ARPES and SARPES experiments are around $50 \mu\text{m}$ and 0.5 mm , respectively, the photoelectron characterization represents an average over the two types of terraces.

In Fig. 2 we compare the experimentally determined electronic structures of $\text{Bi}_4\text{Se}_{2.6}\text{S}_{0.4}$ and Bi_2Se_3 . The bismuth core level ($5d$) spectra [Fig. 2(a)] show a double peak structure of each spin-orbit split state, clearly indicating two different chemical environments for Bi atoms in $\text{Bi}_4\text{Se}_{2.6}\text{S}_{0.4}$: The lower one is similar to the environment in Bi_2Se_3 , whereas the higher one indicates the more metallic character of the Bi_2 layers. This assignment is in agreement with the PEEM data as these two components display a reversed contrast. The wide-energy range valence band spectra, shown in Figs. 2(b) and 2(c), are generally similar for the two materials, with a nearly rigid-band downshift of ~ 0.4 eV of the $\text{Bi}_4\text{Se}_{2.6}\text{S}_{0.4}$ spectrum relative to Bi_2Se_3 yielding a good general correspondence of the bands. The high intensity feature in the $\text{Bi}_4\text{Se}_{2.6}\text{S}_{0.4}$ spectrum that crosses the Fermi level is the central point of this study—this is the TSS, similar to the one observed in Bi_2Se_3 , but also downshifted, with the Dirac point around 0.54 eV below the Fermi level. This downshift of both the valence bands and the TSS suggests that the Bi_2 layers in this natural superlattice phase donate electrons to the Bi_2Se_3 quintuple layers. A PEEM micrograph taken at ~ 0.5 eV below the Fermi level shows the same contrast as the Se $3d$ core level, suggesting that the TSS measured in ARPES is residing on Se-terminated

TABLE I. Structural characterization of $\text{Bi}_4\text{Se}_{2.56}\text{S}_{0.44}$. Space group $R\bar{3}$ (No. 148), $a = 4.2466(8) \text{ \AA}$, $c = 39.706(7) \text{ \AA}$, 329 unique reflections, R_1 (all reflections) = 0.0457, $wR_2 = 0.0938$, Goodness of fit = 1.109.

Atom	Wyck.	x	y	z	Occ.	U_{11}	U_{33}	U_{12}
Bi (1)	6c	0	0	0.143 90(3)		0.0227(4)	0.0307(6)	0.0114(2)
Bi (2)	6c	2/3	1/3	0.045 05(2)		0.0200(4)	0.0262(6)	0.0100(2)
Se (1)	6c	1/3	2/3	0.083 84(8)		0.0276(9)	0.0340(17)	0.0138(4)
Se (2)	3a	0	0	0	0.56(2)	0.024(2)	0.024(3)	0.0122(10)
S (2)	3a	0	0	0	0.44(2)	0.024(2)	0.024(3)	0.0122(10)

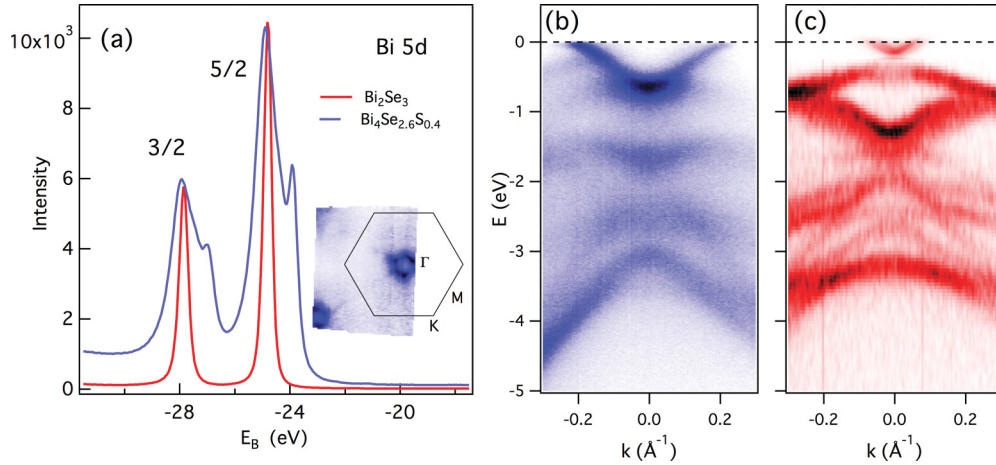


FIG. 2. (Color online) Photoemission spectra from Bi₄Se_{2.6}S_{0.4} and Bi₂Se₃. (a) Bi 5*d* core levels in Bi₄Se_{2.6}S_{0.4} (blue) and Bi₂Se₃ (red). The inset shows the SBZ with the Bi₄Se_{2.6}S_{0.4} Fermi surface measured with 59 eV photons. (b) Valence band along the Γ -*M* line in the SBZ for Bi₄Se_{2.6}S_{0.4} and (c) for Bi₂Se₃.

terraces. A wide k -space survey indicates that the TSS forms a hexagonally shaped Fermi surface at the center of the surface Brillouin zone (SBZ) [Fig. 2(a), inset]. A feature in the valence band spectrum in Fig. 2(b) that does not have an obvious counterpart in the Bi₂Se₃ spectrum is the “holelike” state that crosses with the TSS at $E \approx -0.15$ eV, $k_x \approx \pm 0.15$ \AA^{-1} . This is a bulk state, as will be discussed further with reference to Fig. 3.

In Fig. 3, we show the detailed spin- and k -resolved electronic structure of Bi₄Se_{2.6}S_{0.4}. Figures 3(a) and 3(b) show the photon energy dependence of the ARPES intensity at the Fermi level along the Γ -*K* line and at the center of the SBZ, respectively, for photon energies ranging from 50 to 84 eV in

2 eV steps. The intensity maps are converted into k space by using the inner potential $V = 10$ eV in the approximation for the out-of-plane momentum, $k_z = \frac{1}{\hbar} \sqrt{2m[E_k \cos^2(\theta) + V]}$, where E_k is the kinetic energy of a photoelectron. The straight features at $k_y = \pm 0.173$ \AA^{-1} in Fig. 3(a) represent the Fermi surface of the TSS. The bulk hole state previously mentioned is visible here for negative k_y as a slightly dispersing (with k_z) feature, intertwined around the TSS. The straight vertical line of high intensity in Fig. 3(b) corresponds to the Dirac point of the TSS. Slightly lower in energy, another bulk state can be seen as dispersing with k_z , with the minimum around $k_z = 4.35$ \AA^{-1} . Both bulk features have a periodicity of ≈ 0.5 \AA^{-1} , suggesting that the relevant periodicity in real space

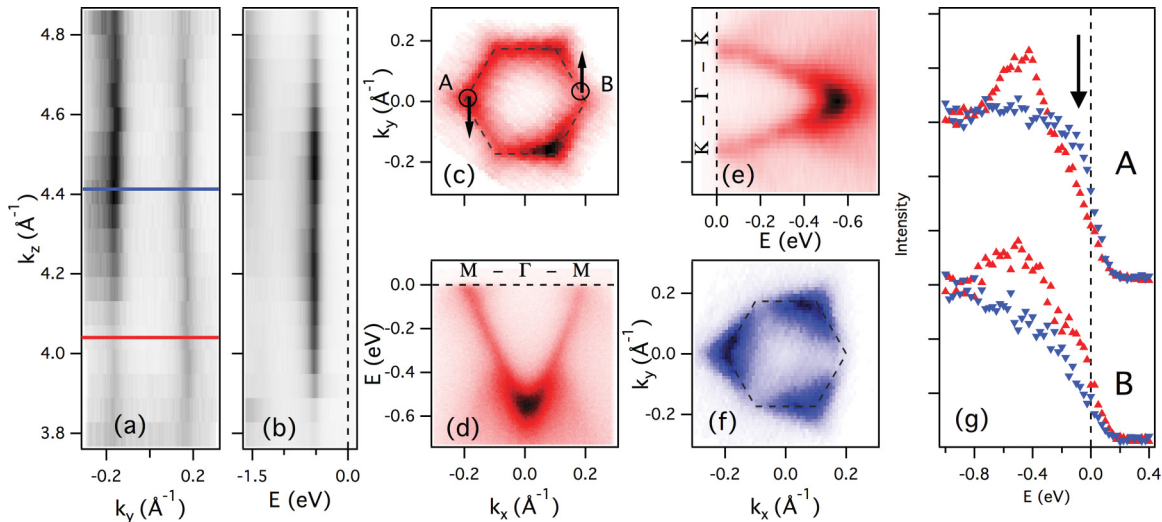


FIG. 3. (Color online) Spin-resolved electronic structure of Bi₄Se_{2.6}S_{0.4}. (a) ARPES intensity at the Fermi level as a function of the in-plane (k_y , along the Γ -*K* line) and out-of-plane (k_z) momentum. (b) Intensity at the Γ point ($k_x = k_y = 0$) of the SBZ as a function of k_z . (c) In-plane Fermi surface measured at $k_z = 4.06$ \AA^{-1} and (f) at $k_z = 4.43$ \AA^{-1} , corresponding to the red and blue lines in (a), respectively. The circles A and B in (c) indicate the k positions where the spin-resolved measurements were performed, while arrows represent the in-plane spin polarization. Dispersion of the surface state along the Γ -*M* (d) and Γ -*K* (e) momentum lines in the SBZ, measured at $k_z = 4.06$ \AA^{-1} . (g) SARPES spectra taken at A and B points in the SBZ, as indicated in (c). Red (blue) spectra represent spin-up (spin-down) components in the y direction. TSS is indicated by the arrow.

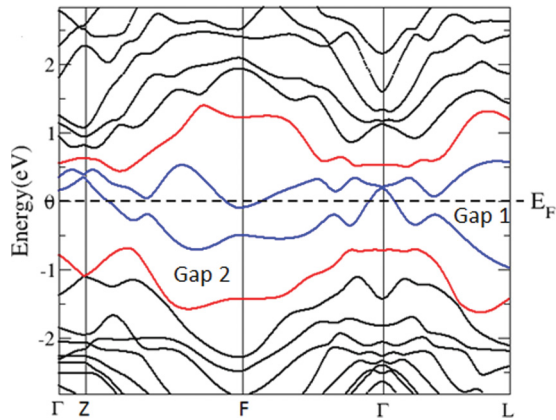


FIG. 4. (Color online) Bulk electronic band structure of Bi_4Se_3 . Colored bands are described in the text.

in the z direction is $\approx 12.5 \text{ \AA}$. This is close to the thickness of one of the $\text{Bi}_2\text{-Bi}_2\text{Se}_3$ composite layers that repeats three times to form the rhombohedral unit cell [Fig. 1(a)]. In Figs. 3(c) and 3(f), we also show the in-plane ARPES intensity at the Fermi level for two photon energies, $h\nu = 58$ and 72 eV , corresponding to $k_z = 4.06$ and 4.43 \AA^{-1} , respectively. The hexagonally shaped contour represents the Fermi surface of the TSS. The dispersion of the surface state measured at $h\nu = 58 \text{ eV}$ along two high symmetry directions in the SBZ is shown in Figs. 3(d) and 3(e). At $h\nu = 72 \text{ eV}$, the intensity at the Fermi level is strongly modulated by the nearly overlapping bulk state with the threefold symmetry [Fig. 3(f)]. The area enclosed by the TSS's Fermi surface is almost an order of magnitude larger than that in pristine Bi_2Se_3 , reflecting a surface electron concentration of $\sim 8.7 \times 10^{12} \text{ cm}^{-2}$. Such high surface electron doping can also be obtained on Bi_2Se_3 through adsorption of various metals on its surface, producing a very similar hexagonal warping of the TSS's Fermi surface.¹⁸

Figure 3(g) shows the spin-resolved spectra with polarization defined in the y direction for points A and B from Fig. 3(c). The peak at the Fermi level, corresponding to the TSS, shows a significant spin polarization ($\sim 30\%$) that reverses sign when the momentum is reversed ($k_x \rightarrow -k_x$), an indication of the chiral spin structure. It is interesting to note that the chirality is opposite to that observed in Bi_2Se_3 .⁸ The peak at around -0.5 eV also shows a polarization, but without the sign reversal, an effect also observed in the bulk valence band in Bi_2Se_3 .¹⁵ The polarization of the TSS is much smaller in $\text{Bi}_4\text{Se}_{2.6}\text{S}_{0.4}$ than in Bi_2Se_3 ,⁸ probably due to the partial overlap with the bulk states or with the Bi_2 -derived states.

Figure 4 shows the calculated bulk band structure of Bi_4Se_3 . SOC plays a significant role as, for example, the lower red colored band has shifted by about 1 eV on the inclusion of SOC. The calculations predict Bi_4Se_3 to be a semimetal with hole pockets at Γ and Z and an electron pocket at F . The hole pockets at Γ and Z project to the $\bar{\Gamma}$ point in the SBZ and are seen in the ARPES measurement. The electron pocket predicted at the bulk F point is not observed by ARPES, suggesting that it lies higher in energy than is predicted by the calculations. Comparison with the Bi_2Se_3 band structure allows us to generally identify bands closely above and below E_F in Bi_4Se_3 as being Bi_2Se_3 -like bands that have been

modified through interactions with the Bi bilayers; these are shown as red in the figure. Bands appearing directly around E_F (blue) in Bi_4Se_3 are primarily Bi_2 -derived states modified by hybridization with the Bi_2Se_3 layers.

There are two continuous gaps in the electronic structure for Bi_4Se_3 , labeled as Gap 1 and Gap 2 in Fig. 4. Counting all bands to Gap 1 gives, for the time-reversal-invariant momenta (TRIM) points of the bulk BZ,³⁰ positive parity for Γ , Z , and L , and negative parity for F . Therefore in Bi_4Se_3 we expect a TSS cone at the projection of the F point in the SBZ. According to the band structure calculation, the cone would be about 0.5 eV below the Fermi energy (for $\text{Bi}_4\text{Se}_2\text{S}$ we expect a second cone at the projection of the Z point, which also has negative parity, but since this would be above the Fermi level it would not be seen by ARPES). Counting the bands until Gap 2 yields, for both Bi_4Se_3 and $\text{Bi}_4\text{Se}_2\text{S}$, TRIM points Z , M , and L with positive parity and Γ with negative parity. This would yield a TSS cone at 0.5 eV below the Fermi level at Γ . Note that counting to Gap 2 is equivalent to counting to the lower red band belonging to Bi_2Se_3 ; we observe the same parity at each TRIM, as is seen in pure Bi_2Se_3 . When counting to Gap 1 one counts to a band belonging to the Bi bilayer. The second cone at F might belong to the Bi_2 , which was predicted to be a 2D quantum spin Hall system.²¹ The crystal cleaves to expose Bi_2 and Bi_2Se_3 Se-terminated terraces, neither of which are at a bulk inversion center. In this case the projection of the bulk BZ points to the surface BZ is less certain, but since the only TRIM at the surface BZ are at $\bar{\Gamma}$ and \bar{M} , the TSS must be at either of those two points. In ARPES we see one TSS cone at $\bar{\Gamma}$ and no cone at \bar{M} [Fig. 2(a), inset]. Where these surface states reside, i.e., on the Bi_2 terraces, the Bi_2Se_3 terraces, or both, and their relation to the bulk band structure, should be the subject of further study on this material.

$\text{Bi}_4\text{Se}_{2.6}\text{S}_{0.4}$ opens several interesting possibilities for studying the role of dimensionality in topological systems: As Fig. 3 shows, there is a 2D n -type TSS, nearly overlapping with a p -type bulk (3D) Fermi surface. In addition, PEEM images from Fig. 1 show alternating Bi_2 -Se terminations, each kind of surface no doubt displaying a different surface electronic structure. Each step would then represent a boundary (or a junction) between two 2D (topological-“trivial” or topological-topological, n - n or p - n) electronic “gases.” This offers the possibility for studying topological phenomena ranging from 1D to 2D to 3D in a single system. The current ARPES experiments lack the necessary spatial resolution to observe such effects, but scanning tunneling microscopy, for example, could provide information about these phenomena. A recent study of a deposited Bi bilayer on Bi_2Te_3 (Ref. 22) has indicated that similar phenomena might be at play in that system: By depositing bismuth, a holelike state is added to the Bi_2Te_3 bands. Although the authors consider the Bi_2 layer to be homogeneous, it might be that terraces with mixed termination are formed in that case as well, creating a situation that is similar to what we observe in $\text{Bi}_4\text{Se}_{2.6}\text{S}_{0.4}$.

We acknowledge helpful discussions with B. A. Bernevig and C. Fang. The work at Brookhaven is supported by the US Department of Energy (DOE) under Contract No. DE-AC02-98CH10886. The work at Princeton University was

supported by SPAWAR Grants No. N66001-11-1-4110 and No. NSF DMR-0819860, and H.W.J. thanks ConocoPhillips

for fellowship support. ALS is operated by the US DOE under Contract No. DE-AC03-76SF00098.

*valla@bnl.gov

†rcava@princeton.edu

- ¹L. Fu, C. L. Kane, and E. J. Mele, *Phys. Rev. Lett.* **98**, 106803 (2007).
- ²H.-J. Noh, H. Koh, S.-J. Oh, J.-H. Park, H.-D. Kim, J. D. Rameau, T. Valla, T. E. Kidd, P. D. Johnson, Y. Hu *et al.*, *Europhys. Lett.* **81**, 57006 (2008).
- ³D. Hsieh, D. Qian, L. Wray, Y. Xia, Y. S. Hor, R. J. Cava, and M. Z. Hasan, *Nature (London)* **452**, 970 (2008).
- ⁴H. Zhang, C.-X. Liu, X.-L. Qi, X. Dai, Z. Fang, and S.-C. Zhang, *Nat. Phys.* **5**, 438 (2009).
- ⁵D. Hsieh, Y. Xia, L. Wray, D. Qian, A. Pal, J. H. Dil, J. Osterwalder, F. Meier, G. Bihlmayer, C. L. Kane *et al.*, *Science* **323**, 919 (2009).
- ⁶Y. Xia, D. Qian, D. Hsieh, L. Wray, A. Pal, H. Lin, A. Bansil, D. Grauer, Y. S. Hor, R. J. Cava *et al.*, *Nat. Phys.* **5**, 398 (2009).
- ⁷Y. L. Chen, J. G. Analytis, J.-H. Chu, Z. K. Liu, S.-K. Mo, X. L. Qi, H. J. Zhang, D. H. Lu, X. Dai, Z. Fang *et al.*, *Science* **325**, 178 (2009).
- ⁸Z.-H. Pan, E. Vescovo, A. V. Fedorov, D. Gardner, Y. S. Lee, S. Chu, G. D. Gu, and T. Valla, *Phys. Rev. Lett.* **106**, 257004 (2011).
- ⁹S. Xu, L. Wray, Y. Xia, R. Shankar, A. Petersen, A. Fedorov, H. Lin, A. Bansil, Y. Hor, D. Grauer *et al.*, arXiv:1007.5111.
- ¹⁰Z. Ren, A. A. Taskin, S. Sasaki, K. Segawa, and Y. Ando, *Phys. Rev. B* **82**, 241306 (2010).
- ¹¹H. Ji, J. M. Allred, M. K. Fuccillo, M. E. Charles, M. Neupane, L. A. Wray, M. Z. Hasan, and R. J. Cava, *Phys. Rev. B* **85**, 201103(R) (2012).
- ¹²K. Nakayama, K. Eto, Y. Tanaka, T. Sato, S. Souma, T. Takahashi, K. Segawa, and Y. Ando, arXiv:1206.7043.
- ¹³T. Sato, K. Segawa, H. Guo, K. Sugawara, S. Souma, T. Takahashi, and Y. Ando, *Phys. Rev. Lett.* **105**, 136802 (2010).
- ¹⁴Y. L. Chen, Z. K. Liu, J. G. Analytis, J.-H. Chu, H. J. Zhang, B. H. Yan, S.-K. Mo, R. G. Moore, D. H. Lu, I. R. Fisher *et al.*, *Phys. Rev. Lett.* **105**, 266401 (2010).
- ¹⁵C. Jozwiak, Y. Chen, A. Fedorov, J. Analytis, C. Rotundu, A. Schmid, J. Denlinger, Y.-D. Chuang, D.-H. Lee, I. Fisher *et al.*, *Phys. Rev. B* **84**, 165113 (2011).
- ¹⁶M. Bianchi, R. C. Hatch, J. Mi, B. B. Iversen, and P. Hofmann, *Phys. Rev. Lett.* **107**, 086802 (2011).
- ¹⁷H. M. Benia, C. Lin, K. Kern, and C. R. Ast, *Phys. Rev. Lett.* **107**, 177602 (2011).
- ¹⁸T. Valla, Z.-H. Pan, D. Gardner, Y. S. Lee, and S. Chu, *Phys. Rev. Lett.* **108**, 117601 (2012).
- ¹⁹Z.-H. Pan, A. V. Fedorov, D. Gardner, Y. S. Lee, S. Chu, and T. Valla, *Phys. Rev. Lett.* **108**, 187001 (2012).
- ²⁰H. Lind and S. Lidin, *Solid State Sci.* **5**, 47 (2003).
- ²¹S. Murakami, *Phys. Rev. Lett.* **97**, 236805 (2006).
- ²²T. Hirahara, G. Bihlmayer, Y. Sakamoto, M. Yamada, H. Miyazaki, S.-I. Kimura, S. Blügel, and S. Hasegawa, *Phys. Rev. Lett.* **107**, 166801 (2011).
- ²³P. Blaha, K. Schwarz, G. Madsen, D. Kvasnicka, and J. Luitz, *WIEN2k, An Augmented Plane Wave + Local Orbitals Program for Calculating Crystal Properties* (Technische Universität Wien, Austria, 2001).
- ²⁴D. J. Singh and L. Nordström, *Planewaves, Pseudopotentials, and the LAPW Method*, 2nd ed. (Springer, New York, 2006).
- ²⁵G. K. H. Madsen, P. Blaha, K. Schwarz, E. Sjöstedt, and L. Nordström, *Phys. Rev. B* **64**, 195134 (2001).
- ²⁶E. Sjöstedt, L. Nordström, and D. J. Singh, *Solid State Commun.* **114**, 15 (2000).
- ²⁷J. P. Perdew, K. Burke, and M. Ernzerhof, *Phys. Rev. Lett.* **77**, 3865 (1996).
- ²⁸M. M. Stasova, *Izv. Akad. Nauk SSSR* **4**, 28 (1968).
- ²⁹L. Vegard, *Z. Phys. A: Hadrons Nucl.* **5**, 17 (1921).
- ³⁰L. Fu and C. L. Kane, *Phys. Rev. B* **76**, 045302 (2007).